Dyes and Pigments 185 (2021) 108899

Contents lists available at ScienceDirect

Dyes and Pigments

journal homepage: http://www.elsevier.com/locate/dyepig

Impact of the acceptor units on optoelectronic and photovoltaic properties of $(XDADAD)_n$-type copolymers: Computational and experimental study

Irina V. Klimovich [a,b,*], Fedor A. Prudnov [a,b], Olga Mazaleva [a], Nikita V. Tukachev [a], Alexander V. Akkuratov [b], Ilya V. Martynov [b], Alexander S. Peregudov [c], Alexander F. Shestakov [b], Andriy Zhugayevych [a], Pavel A. Troshin [a,b]

[a] Skolkovo Institute of Science and Technology, Bolshoy Boulevard 30, Bld. 1, Moscow, 121205, Russian Federation
[b] Institute of Problems of Chemical Physics of Russian Academy of Sciences Academician, Semenov Avenue 1, Chernogolovka, Moscow Region, 142432, Russian Federation
[c] A.N.Nesmeyanov Institute of Organoelement Compounds of Russian Academy of Sciences, Vavilova St. 28, Moscow, 119991, Russian Federation

ARTICLE INFO

Keywords:
Organic solar cell
Conjugated polymers
Acceptor block
Quinoxaline
Benzotriazole

ABSTRACT

A series of ten conjugated polymers incorporating in their molecular frameworks extended DADAD building blocks with thiophene donor (D) and either benzotriazole, benzoxadiazole, benzothiadiazole, difluorobenzothiadiazole or quinoxaline acceptor (A) units were synthesized and characterized. The optoelectronic properties of new polymers were computed and experimentally investigated revealing a good relationship, which can guide further rational design of materials with tailored properties for organic photovoltaics using *in-silico* approaches. The performance of all polymers in organic bulk heterojunction solar cells was compared and some important empirical rules were formulated for reaching the best photovoltaic performance from $(X\text{-}DADAD)_n$ family of polymers.

1. Introduction

The progress of organic photovoltaics is generally fueled by the development of new donor-acceptor conjugated polymers. A huge number of possible combinations of donor and acceptor building blocks allows one to optimize thoroughly all functional properties of polymers [1,2].

A common approach to the rational design of conjugated polymers is based on the combination of a weak donor and a strong acceptor in a polymer chain [3]. Since the donor block has a greater influence on the position of HOMO (the highest occupied molecular orbital) energy level, inclusion of blocks with weaker donor properties increases the open-circuit voltage (V_{OC}) in solar cells [4]. The variation of the acceptor block allows to change the LUMO (the lowest unoccupied molecular orbital) energy level, adjusting the band gap of the polymer and, thus, influencing the short-circuit current density (J_{SC}) of the device [5]. Balancing the gains and losses in J_{SC} and V_{OC} by systematic screening of hundreds of donor and acceptor combinations delivered the light power conversion efficiencies over 11% for solar cells based on polymer-fullerene systems [6–8]. Even higher efficiencies of up to ~18% were recently reported for optimized organic solar cells comprising non-fullerene acceptors [9]. Notably, despite huge variety of donor blocks, the design of acceptor blocks and investigation of their influence on the properties of resulting polymers received only limited attention.

A promising approach to design conjugated polymers with desired characteristics is based on incorporation of extended D_1-A-D_2-A-D_1 blocks in their molecular frameworks. It allows one to tune optoelectronic and physicochemical properties of these materials by combination of various D_1, D_2 and A units. Moreover, these structures ensure regioregularity of the resulting polymers in case of using nonsymmetrical blocks such as thiadiazolo [3,4-c]pyridine, 5-fluoro-2,1,3-benzothiadiazole, etc. [10,11].

The $(X\text{-}DADAD)_n$-type conjugated polymers demonstrated impressive photostability in both thin films and solar cells suggesting that operation lifetimes of 10–15 years are feasible for these materials [12–14]. The efficiencies of the solar cells based on such donor polymers and fullerene acceptors go beyond 7% for spin-coated devices and reach over 6% for larger-area cells processed in ambient air using Doctor blade or slot die coating techniques [15]. The later aspect is especially

* Corresponding author. Skolkovo Institute of Science and Technology, Bolshoy Boulevard 30, bld. 1, Moscow, 121205, Russian Federation.
E-mail address: irina.v.klimovich@gmail.com (I.V. Klimovich).

https://doi.org/10.1016/j.dyepig.2020.108899
Received 6 July 2020; Received in revised form 21 September 2020; Accepted 29 September 2020
Available online 1 October 2020

important for commercial applications of organic photovoltaics. Small molecules with similar structural DADAD motif demonstrated good performance in solar cells with the efficiencies approaching 8% in combination with both fullerene [16] and non-fullerene acceptors [17].

In this work, we investigated the impact of the acceptor blocks on the optoelectronic properties of $(X\text{-DADAD})_n$-type conjugated polymers and their performance in solar cells. In particular, the known family of such polymers was expanded by using functionalized benzotriazole, quinoxaline and bis(octyloxy)benzothiadiazole as acceptor units (Fig. 1). We compared properties of these materials with the previously reported polymers incorporating benzothiadiazole, fluorinated benzothiadiazole and benzoxadiazole as A units [12,18–20]. Using computational and experimental approaches we establish relationship between the structure of polymers (particularly, the type of the used A unit), their optoelectronic properties, morphological behavior in thin films and photovoltaic characteristics.

2. Results and discussion

2.1. Synthesis of polymers

The approach used for the synthesis of target conjugated polymers are shown in Scheme 1. Dibrominated derivatives of quinoxaline, bis(octyloxy)benzothiadiazole and benzotriazole were prepared following standard procedures [21,22]. The preparation of key DADAD blocks was based on the initial Stille coupling between the dibrominated acceptor block BrABr and tributyl (thiophen-2-yl)stannane to form DABr derivatives, that were further treated with 2,5 bis(tributhylstannyl)thiophene to obtain oligomers **A3-A8**.

The bromination of **A3-A8** with 2 eq. of N-bromosuccinimide (NBS) followed by cross-coupling of **B3**–**B5** and **B8** with tributyl (thiophen-2-yl)stannane or Suzuki reaction of **B6** or **B7** with (3-(2-ethylhexyl)thiophen-2-yl)boronic acid resulted in compounds **C3**–**C8**. Finally, bromination of **C3**–**C8** with NBS afforded **D3-D8**. The synthesis of **P3**–**P8** was performed under standard Suzuki-Miyaura polycondensation reaction conditions using carbazole-based diboronic component [23]. The synthesized polymers were subsequently purified by Soxhlet extraction

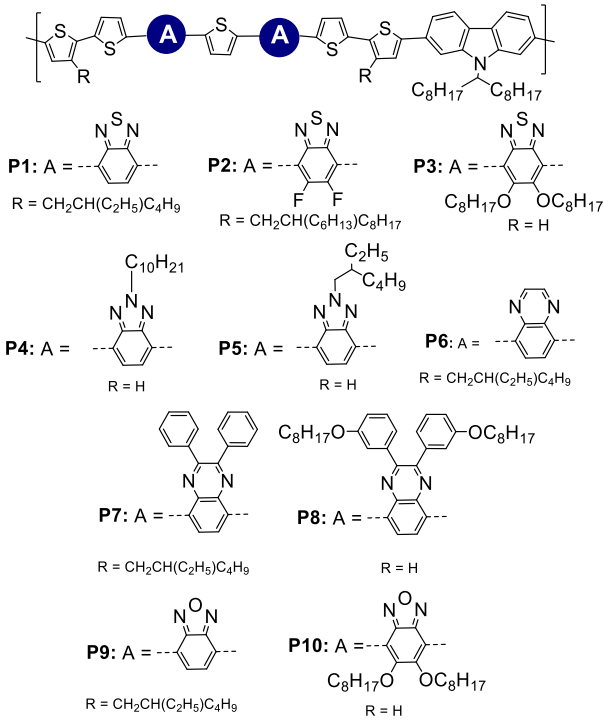

Fig. 1. Chemical structures of the investigated polymers **P1**–**P10**.

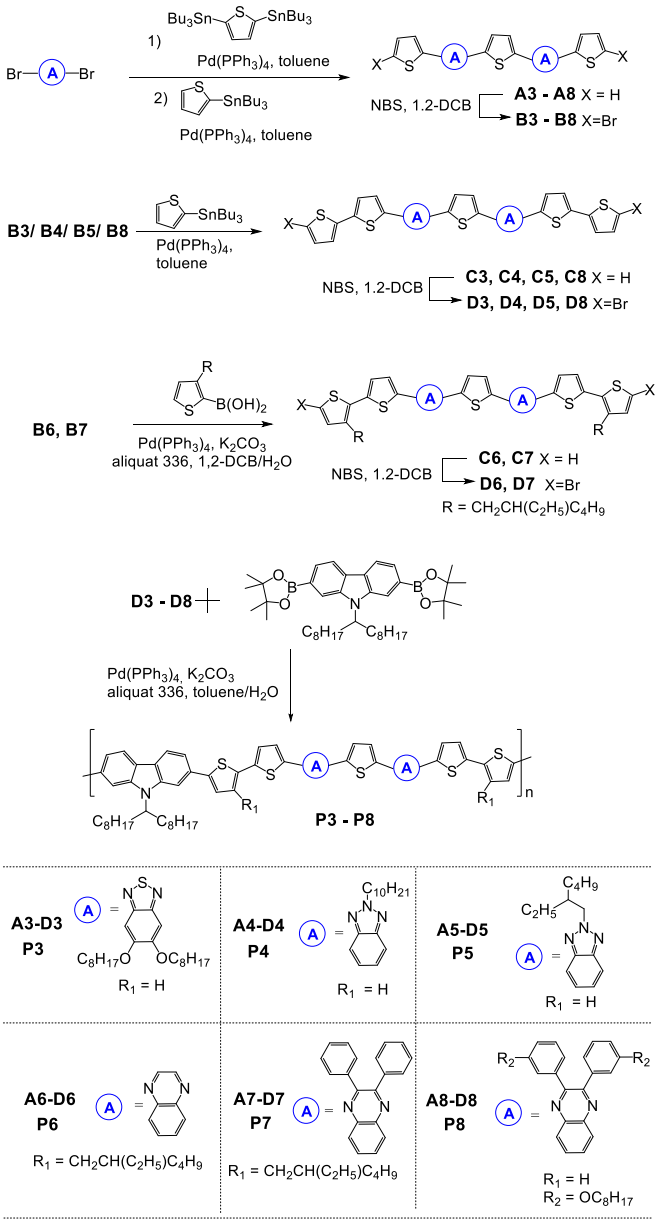

Scheme 1. Synthesis of polymers **P3**–**P8**.

with acetone, heptane, dichloromethane and chlorobenzene.

The corresponding extracts (usually with chlorobenzene) were concentrated and precipitated in methanol. Relative molecular weight

Table 1
Characteristics of polymers **P1**–**P10**.

Polymer	M_w, kDa	M_w/M_n	E_g^{opt}, eV	E_{onset}^{ox} *vs* Fc/Fc^+, V	$HOMO_{el}$, eV	LUMO, eV[a]
P1	201	4.0	1.66	0.34	−5.44	−3.78
P2	132	2.9	1.70	0.49	−5.59	−3.89
P3	41	1.2	1.84	0.43	−5.54	−3.66
P4	49	2.1	2.01	0.38	−5.48	−3.47
P5	38	1.9	1.97	0.41	−5.51	−3.48
P6	81	8.8	1.80	0.36	−5.46	−3.65
P7	109	2.4	1.80	0.34	−5.44	−3.63
P8	82	6.4	1.81	0.45	−5.55	−3.74
P9	97	6.8	1.63	0.35	−5.44	−3.81
P10	31	4.7	1.86	0.42	−5.52	−3.69

[a] LUMO levels were calculated as E (HOMO)+.E_g^{opt}

characteristics of the obtained polymers determined by the gel permeation chromatography (GPC) method are given in Table 1.

2.2. Optoelectronic properties

UV–visible absorption spectra of polymers in thin films are shown in Fig. 2a. All polymers demonstrate two wide absorption bands in the range of 400–800 nm. In terms of the optical band gap E_g^{opt} estimated from the low energy absorption onset, all polymers can be divided into three groups. The first one includes polymers incorporating benzotriazole blocks (**P4, P5**), which have wide band gap of ~2 eV. Benzotriazole demonstrates weak electron acceptor properties because the lone pair of alkyl-substituted nitrogen atom is strongly coupled with triazole aromatic ring. Another group of materials with a band gap of about 1.8 eV is formed by polymers with quinoxaline or alkoxysubstituted benzoxadiazole and benzothiadiazole units (**P3**, **P6, P7, P8, P10**). Finally, polymers **P1, P2** and **P9** based on unsubstituted benzothiadiazole, difluorobenzothiadiazole and benzoxadiazole exhibit the lowest band gaps of ~1.6 eV.

Electrochemical properties of polymers were investigated using cyclic voltammetry (Fig. 2b). HOMO energy levels were estimated based on the onsets of the oxidation peaks with the assumption that the Fc/Fc^+ couple has Fermi energy of −5.10 eV [24] (Table 1). Since HOMO is mostly defined by the donor building block, any noticeable changes in the HOMO energy can be induced only by those acceptor units, which have a strong electron withdrawing ability (**P2**).

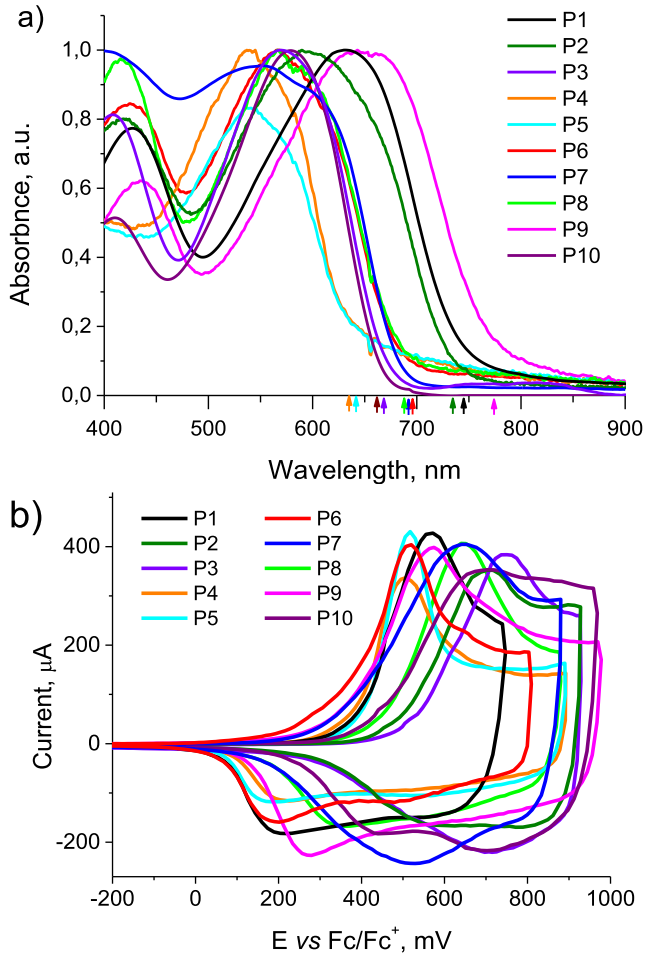

Fig. 2. Absorption spectra (a) and cyclic voltammograms (b) of polymers **P1**–**P10** in thin films. The arrows indicate the wavelengths of the absorption edges used to determine E_g for corresponding polymer.

Surprisingly, introduction of alkoxy groups on the acceptor unit also leads to the decrease in HOMO energy levels (**P3**, **P10**). However, this effect is mostly related to increase in the material band gap presumably because of reduced conjugation length enabled by changes in the polymer chain geometry due to introduction of bulky alkoxy substituents.

The LUMO energy levels of polymers **P1–P10** were calculated as E (HOMO)+ E_g^{opt} since no well-shaped reduction peaks were observed on cyclic voltammograms. The LUMO(polymer) - LUMO(acceptor) offset should be sufficient to overcome the exciton binding energy and provide a necessary driving force for efficient photoinduced charge separation in the polymer/fullerene blends [25]. Considering the values given in Table 1, one can notice that LUMO energies of **P1–P10** are considerably higher compared to that of the fullerene acceptors $PC_{61}BM$ (−4.1 eV) [26] and $PC_{71}BM$ (−3.9 eV) [27] (Table 1).

2.3. Theoretical studies

To rationalize the experimentally revealed optoelectronic properties of the polymers and elucidate the nature of frontier electronic states and optical transitions, we performed DFT calculations for long enough oligomers simulating the structures of **P1–P10** (with removed aliphatic substituents). More specifically, DFT allowed us to estimate excitation energies, ionization potentials (IPs) and electron affinities (EAs) as well as frontier orbitals energies. In particular, the calculations of the excited states assign the lowest energy absorption band to intramolecular charge transfer between the donor and acceptor units, whereas the higher energy band corresponds mainly to the π-π* electron transition in the polymer backbone, see Fig. 3a for **P2** and Figs. S1–S2 in ESI for other polymers. Very similar IP values were expected for these polymers due to virtually the same HOMO structure (Fig. S2). A clear correlation between the optical bandgap, which is one of the key experimentally determined parameters, and the theoretically estimated HOMO-LUMO

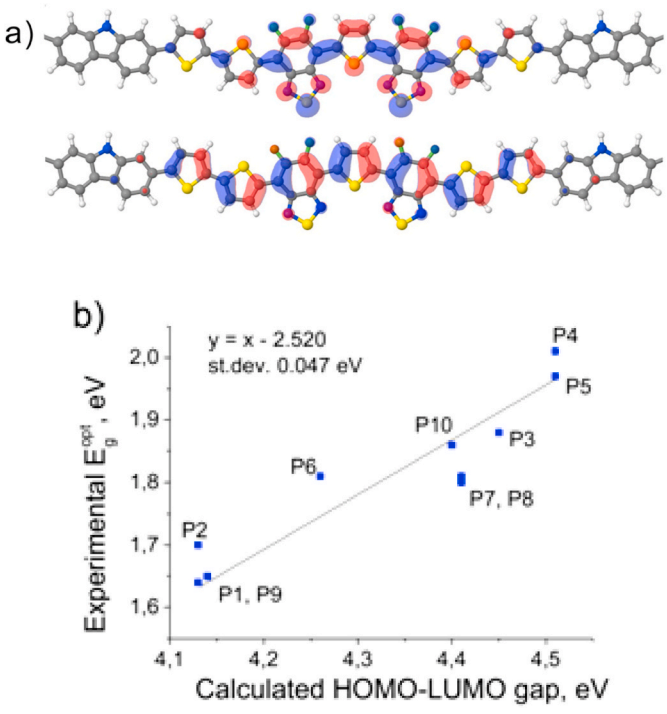

Fig. 3. (a) Natural transition orbitals for the fragment of **P2** polymer chain (electron NTO - top, hole NTO - bottom) (b) Correlation between HOMO-LUMO gap (CAM-B3LYP/6-31G*) and optical absorption energy of **P1**–**P10**. Solid black line is a linear fit with a constraint (slope must be equal to 1) for this data set. Linear regression equation, as well as standard deviation, are given in the top-left corner.

energy difference for model oligomers was observed (Fig. 3b). Comparing this with the correllations presented in Fig. S3 and Fig. S4 (ESI), one might come to a conclusion that, at least for the investigated polymer series, errors introduced by overaccounting the exchange interactions or accounting for solvation effects affect primarily the intercept term in the linear regression equation, which was used to fit the data points in Fig. 3b.

Thus, from the perspective of theoretical modelling of the polymer structure, the simplified approach dealing with just frontier orbitals might be used. However, there seem to be no notable correlation between the experimentally estimated HOMO energy values and computed ionization potentials (Fig. S5). In quantum chemistry calculations ionization potential and electronic excitation energies should be estimated as an energy difference of cation (or excited state) and neutral molecule. In this work, it is shown that HOMO energy (HOMO-LUMO gap) could be used as scalable alternatives when analyzing relative trends for a series of similar compounds. Theoretical results obtained in these two approaches show solid correlations for IP (Fig. S6). Thus, the relatively computationally inexpensive approach used in this work allows one to predict band gaps for a set of similar conjugated polymers and has a potential to be used as a tool for digging out new promising structures. However, both experimentally and theoretically predicted ionization potentials for that similar structures could not be used as a reliable descriptor for selection of the most appropriate polymer structures.

Examining polymer NTOs (Fig. 3a), one could see that there is zero density on carbazole unit. Apparently this effect could not be correctly described by one-electron approximation and thus HOMO does not represent this over-localization (Fig. S10). Analyzing localized MO interactions (Figs. S11–S12), one can see that carbazole orbitals participating in conjugation and facilitating intramolecular charge transfer (those with energies −9.50 and −7.49 eV) have relatively small electronic couplings (0.54 and 0.42, respectively) as compared to those between other fragments (Table S5). However, analyzing hole NTO localization for a set of similar structures (Fig. S13), one could easily see that the density is redistributed between 7 fragments in almost identical way regardless of carbazole position; thus this localization should be mainly attributed to size effects rather than small electron couplings between carbazole and thiophene.

2.4. Photovoltaic properties

The designed conjugated polymers were studied in organic solar cells as electron donor components in combination with the fullerene-based acceptor material phenyl-C71-butyric acid methyl ester ($PC_{71}BM$). The assembled devices had the following configuration: glass/ITO/PEDOT:PSS/polymer: $PC_{71}BM$ blend/Mg/Al [28]. The optimization of the devices included variations in the ratio of fullerene and polymer components in the composite, solvent used for film coating, additive and its concentration, annealing regimes, and thickness of the film. The optimum conditions are given in Table 2. The current-voltage characteristics and EQE spectra are shown in Fig. 4.

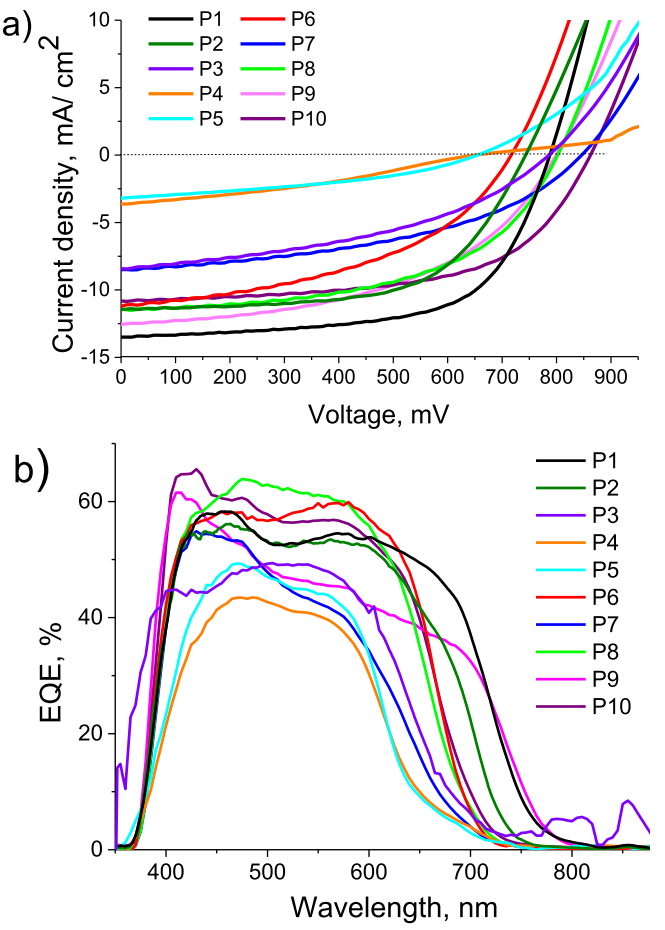

Fig. 4. a) *J*-V curves measured under simulated AM1.5 (100 mW cm^{-2}) illumination and b) EQE spectra for the solar cells based on composites of polymers **P1**–**P10** with $PC_{71}BM$.

Polymers **P4** and **P5** with benzotriazole acceptor blocks showed the lowest light power conversion efficiencies (PCEs) of 1.6% and 1.8%, respectively. Low values of J_{SC}, which amount only to 20–25% of the maximum achievable values (J_{SC}^{max}) calculated based on the band gap (Table S1), and inferior EQE values of <50% imply that the efficiency of the devices is limited mainly by recombination losses. Indeed, polymers **P4** and **P5** showed poor miscibility with the acceptor fullerene derivatives leading to large-scale phase segregation in the films as can be concluded from the topography images shown in Fig. 5 and obtained using atomic force microscopy (AFM). It is known that exciton diffusion lengths in organic semiconductors stay within the range of 5–20 nm [29]. Therefore, formation of large domains of pure materials in the composite films leads to massive exciton recombination and, hence,

Table 2
Processing conditions and parameters of organic solar cells based on the blends of polymers **P1**–**P10** with $PC_{71}BM$.

	D/A ratio	Solvent	Annealing regime[a]	Rotation speed, rpm	V_{OC}, mV	J_{SC}, mA cm^{-2}	FF,%	η,%	Data source
P1	1:2	1,2-DCB with 0.63% of 1,8-DIO	10 min at 90 °C	900	775	13.6	62	6.4	[12]
P2	1:2.5	1,2-DCB with 0.312% of 1,8-DIO	10 min at 95 °C	1100	743	11.4	61	5.2	[18]
P3	1:2	1,2-DCB	10 min at 95 °C	1800	800 ± 20	7.6 ± 0.2	43 ± 2	2.6 ± 0.2	This work
P4	1:1	1,2-DCB	10 min at 95 °C	600	640 ± 10	5.4 ± 0.6	41 ± 2	1.4 ± 0.2	This work
P5	1:2	1,2-DCB	10 min at 95 °C	600	615 ± 15	6.3 ± 0.1	41 ± 3	1.6 ± 0.2	This work
P6	1:1	1,2-DCB	15 min at 90 °C	1400	693 ± 26	10.1 ± 1.1	41 ± 4	3.2 ± 0.4	This work
P7	1:1	1,2-DCB	10 min at 110 °C	700	840 ± 6	8.3 ± 0.2	44 ± 3	3.1 ± 0.2	This work
P8	1:1	1,2-DCB	10 min at 95 °C	700	809 ± 19	11.4 ± 0.1	52 ± 4	4.8 ± 0.1	This work
P9	1:2	Chlorobenzene with 0.3% of 1-CN	10 min at 90 °C	1700	800	12.6	49	4.9	[19]
P10	1:2	1,2-DCB with 1.25% of 1-CN	10 min at 95 °C	1600	862	10.8	59	5.5	[20]

[a] Before electrodes deposition.

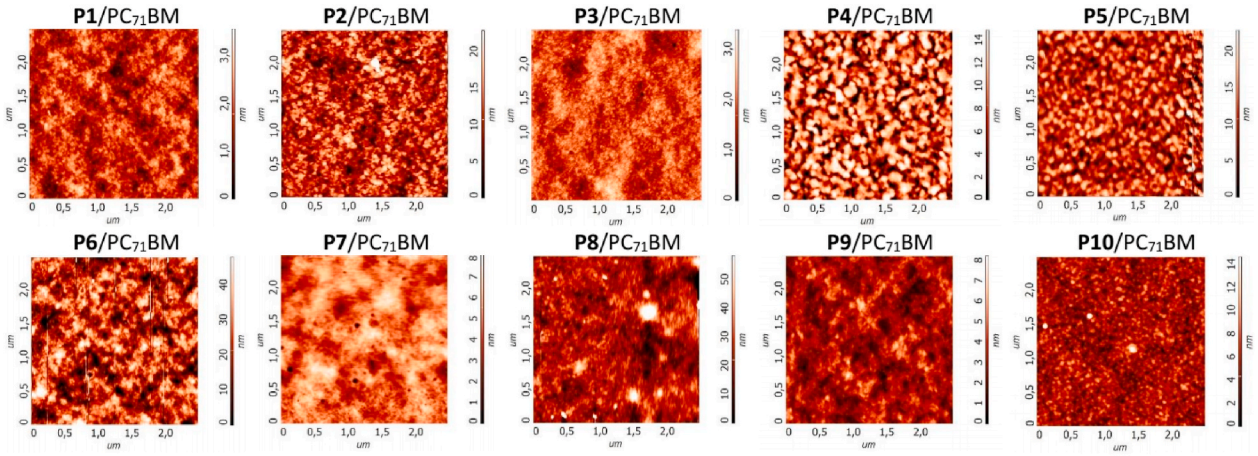

Fig. 5. AFM topography images for thin films of composites of **P1**–**P10** with $PC_{71}BM$ processed as specified in Table 2.

inefficient photocurrent generation. It is very likely that such unfavorable behavior is related to the presence of benzotriazole units in the molecular frameworks of **P4** and **P5** suggesting that they are probably not suitable for designing $(X\text{-}DADAD)_n$-type electron donor polymers for efficient fullerene-based organic solar cells.

On the contrary, the highest current densities were delivered by the devices incorporating polymers **P1**, **P2**, **P6**, and **P8**–**P10**, which also showed balanced nanoscale morphology in composite films with $PC_{71}BM$ (Fig. 5) ensuring efficient charge generation and transport. These results feature substituted or non-substituted benzothiadiazole, benzooxadiazole and quinoxaline units as promising acceptor blocks for designing $(X\text{-}DADAD)_n$ conjugated polymers.

It should be emphasized that we observed no expected correlation [30] between the experimental device open circuit voltages and polymer HOMO energy levels estimated either experimentally from cyclic voltammetry data or computed using theoretical DFT approaches (Table S2, ESI). Indeed, the polymers **P4** and **P5** delivered the lowest V_{OC} values in spite of their deep-lying HOMO levels (ca. −5.5 eV, Table S2, ESI). This discrepancy might be related to non-optimal blend morphology [31] and strong contribution from the charge carrier recombination [32].

We believe that trap-assisted recombination reduces the performance of the solar cells based on polymer **P2** since they show open-circuit voltage of 743 mV in spite of the low HOMO energy of – 5.59 eV. On the contrary, polymers **P7** and **P9** delivered high V_{OC} of 800–850 mV, while their HOMO energy (−5.44 eV) is higher than for all other polymers. This fact might suggest that these two polymers incorporating substituted quinoxaline and benzoxadiazole acceptor units have lower concentration of defects thus suppressing recombination losses.

To summarize, the obtained results suggest that benzothiadiazole and properly functionalized quinoxaline and benzoxadiazole represent the most promising acceptor building blocks for designing $(X\text{-}DADAD)_n$ type copolymers for photovoltaic applications.

3. Conclusions

The $(X\text{-}DADAD)_n$ type polymers comprising alkyl benzotriazoles and quinoxaline derivatives as an electron acceptor unit in combination with thiophene rings as the donor have been synthesized and characterized in detail. Their optoelectronic and photovoltaic properties were compared with previously published results for polymers based on benzothiadiazole and benzoxadiazole derivatives. Introduction of the weak acceptor units result in wider band gaps and lower values of J_{SC} and V_{OC} of solar cells. Moreover, polymers composed of quinoxaline-based building blocks ensure reasonable J_{SC} and/or V_{OC} of devices.

The data obtained in this work, supplemented by previously published results and theoretical calculations, allowed us to design a simple approach for assessing the optoelectronic properties of new structures of $(X\text{-}DADAD)_n$-type polymers.

4. Experimental

4.1. Materials and instrumentation

All solvents and reagents were purchased from Sigma-Aldrich or Acros Organics and used as received or purified according to standard procedures. AFM images were obtained using an NTEGRA PRIMA instrument (NT-MDT, Russia). Absorption spectra (for thin films of polymers) were obtained using an Avantes AvaSpec-2048 optical fiber spectrometer.

Molecular weight characteristics of conjugated polymers were obtained using a Shimadzu LC20 instrument equipped with a Phenomenex Luna Phenogel 5μm column (0.78 × 30 cm, 5–500 kDa). The measurements were performed using freshly distilled toluene as an eluent (flow rate 0.5 mL min^{-1}, column temperature 50 °C). The column was calibrated using a series of custom-made F8BT standards with PDI <1.5 (toluene used as eluent). Molecular weights of the F8BT standards were crosschecked additionally using a "Waters Alliance GPCV 2000" instrument equipped with a multi-angle scattering detector HELEOS II (Wyatt).

Purification of low molecular weight compounds (key building blocks) was performed using preparative GPC at Shimadzu LC20 instrument equipped with a Shodex GPC K-2001 50 Å 6 μm, (20 × 300 mm). Freshly distilled toluene was used as an eluent (flow rate 1 mL min^{-1}, column temperature 40 °C).

4.2. Synthesis of A3-A8

Corresponding dibrominated derivatives of acceptor building blocks (3 eq) and 2-(tributylstannyl) thiophene (1 eq) were dissolved in anhydrous toluene (50 mL) in a three-necked round-bottom flask. The mixture was deaerated and $Pd(PPh_3)_4$ (0.023 g, 0.015 eq) was added under argon. The mixture was heated at reflux for 24 h and then cooled to the room temperature. 2,5-bis(tributylstannyl)thiophene (7 eq) was added and reaction mixture was heated at reflux for another 24 h. After cooling to room temperature, the mixture was washed with water, organic phase collected, dried over $MgSO_4$ and concentrated at the rotary evaporator. The target compounds **A3-A8** were separated from the side products and starting compounds by column chromatography on SiO_2 (light petroleum-toluene mixtures as eluent) and further purified by preparative GPC.

A3 (2,5-bis(5,6-bis(octyloxy)-7-(thiophen-2-yl)benzo[c][1,2,5]thiadiazol-4-yl)thiophene): ^{1}H NMR ($CDCl_3$, 500 MHz): δ (ppm) 8.60 (s, 2H),

8.50 (dd, $J = 4.1$ Hz, 1.2 Hz, 2H), 7.52 (dd, $J = 4.1$ Hz, 1.2 Hz, 2H), 7.25 (m, 2H), 4.15 (m, 8H), 1.95–2.01 (m, 8H), 1.47 (m, 8H), 1.23–1.35 (m, 36H), 0.90 (t, $J = 6.7$ Hz, 6H), 0.83 (t, $J = 6.9$ Hz, 6H) ^{13}C NMR ($CDCl_3$, 126 MHz): δ (ppm) 152.38, 152.24, 151.24, 136.37, 134.38, 130.72, 127.48, 126.93, 118.01, 117.75, 74.59, 74.54, 32.01, 30.61, 30.54, 29.82, 29.71, 29.50, 29.46, 26.20, 26.18, 22.84, 22.80, 14.27, 14.21 Calculated for $C_{56}H_{76}N_4O_4S_5$ C, 65.33; H, 7.44; N, 5.44; O, 6.22; S, 15.57, Found: C 65.02, H 7.52, N 5.51, S 15.48.

A4 (2,5-bis(2-(decyl)-7-(thiophen-2-yl)-2H-benzo[d][1,2,3]triazol-4-yl)thiophene):^{1}H NMR ($CDCl_3$, 500 MHz): δ (ppm) 8.21 (s, 2H), 8.12 (dd, $J = 3.6$, 1.1 Hz, 2H), 7.72 (d, $J = 7.6$ Hz, 2H), 7.66 (d, $J = 7.6$ Hz, 2H), 7.39 (dd, $J = 5.1$, 1.1 Hz, 2H), 7.20 (dd, $J = 5.1$, 3.6 Hz, 2H), 4.85 (t, $J = 7.2$ Hz, 4H), 2.23 (m, 4H), 1.44 (m, 4H), 1.26 (m, 24H), 0.86 (t, $J = 6.8$ Hz, 6H) ^{13}C NMR ($CDCl_3$, 126 MHz): δ (ppm) 142.25, 140.16, 140.06, 128.59, 128.27, 127.15, 125.73, 123.81, 123.67, 122.95, 122.87, 57.04, 32.03, 30.24, 29.68, 29.61, 29.44, 29.22, 26.78, 22.82, 14.26 21 Calculated for $C_{44}H_{54}N_6S_3$: C, 69.25; H, 7.13; N, 11.01; S, 12.60, Found C 69.09, H 7.20, N 10.73, S 12.98.

A5 (2,5-bis(2-(2-ethylhexyl)-7-(thiophen-2-yl)-2H-benzo[d][1,2,3]triazol-4-yl)thiophene): ^{1}H NMR ($CDCl_3$, 500 MHz): δ (ppm) 8.21 (s, 2H), 8.03 (dd, $J = 3.6$, 1.1 Hz, 2H), 7.68 (d, $J = 7.6$ Hz, 2H), 7.61 (d, $J = 7.6$ Hz, 2H), 7.27 (dd, $J = 5.1$, 1.1 Hz, 2H), 7.05 (dd, $J = 5.1$, 3.6 Hz, 2H), 4.78 (d, $J = 7.2$ Hz, 4H), 2.31 (m, 2H), 1.44 (m, 4H), 1.26 (m, 12H), 1.03 (t, $J = 6.8$ Hz, 6H), 0.93 (t, $J = 6.8$ Hz, 6H) ^{13}C NMR ($CDCl_3$, 126 MHz): δ (ppm) 142.25, 140.16, 140.06, 128.59, 128.27, 127.15, 125.73, 123.81, 123.67, 122.95, 122.87, 57.04, 32.03, 30.24, 29.68, 29.61, 29.44, 29.22, 26.78, 22.82, 14.26 Calculated for $C_{40}H_{46}N_6S_3$: C, 67.95; H, 6.56; N, 11.89; S, 13.60, Found C, 68.11; H, 6.70; N, 11.50; S, 13.69.

Compound **A6** (2,5-bis(8-(thiophen-2-yl)quinoxalin-5-yl)thiophene) is not soluble in organic solvents, therefore its characterisation with NMR spectroscopy was not possible. ESI-MS $m/z = 504$, $[M]^+$. FT-IR (KBr): 3453, 1637, 1560, 1523, 1460, 1383, 1337, 1228, 1178, 1100, 1054, 1022, 969, 820, 799, 768, 703, 609, 537 Calculated for $C_{28}H_{16}N_4S_3$ (%) C, 66.64; H, 3.20; N, 11.10; S, 19.06, Found C, 67.14; H, 3.80; N, 11.26; S, 17.8.

A7 (2,5-bis(2,3-diphenyl-8-(thiophen-2-yl)quinoxalin-5-yl)thiophene):^{1}H NMR ($CDCl_3$, 500 MHz): δ (ppm) 8.16 (d, $J = 1.8$ Hz, 4H), 8.00 (s, 2H), 7.89 (dd, $J = 3.7$, 1.1 Hz, 2H), 7.77–7.75 (m, 4H), 7.68–7.66 (m, 4H), 7.50 (dd, $J = 5.0$, 1.2 Hz, 2H), 7.41 (m, 8H), 7.28 (m, 2H), 7.23 (m, 2H), 7.18 (m, 2H), ^{13}C NMR ($CDCl_3$, 126 MHz): δ (ppm) 151.85, 151.75, 141.48, 139.86, 138.70, 138.58, 137.51, 136.83, 131.77, 130.63, 130.58, 130.42, 129.35, 129.27, 129.12, 129.01, 128.40, 128.24, 127.03, 126.01, 124.20, 123.89, 112.08 Calculated for $C_{51}H_{31}N_4S_3$ C, 76.95; H, 3.93; N, 7.04; S, 12.08, Found C, 76.59; H, 4.13; N, 7.17; S, 12.11.

A8 (2,5-bis(2,3-bis(3-(octyloxy)phenyl)-8-(thiophen-2-yl)quinoxalin-5-yl)thiophene):^{1}H NMR ($CDCl_3$, 500 MHz): δ (ppm) 8.21 (s, 2H), 8.12 (dd, $J = 3.6$, 1.1 Hz, 2H), 7.72 (d, $J = 7.6$ Hz, 2H), 7.66 (d, $J = 7.6$ Hz, 2H), 7.39 (dd, $J = 5.1$, 1.1 Hz, 2H), 7.20 (dd, $J = 5.1$, 3.6 Hz, 2H), 4.85 (t, $J = 7.2$ Hz, 4H), 2.23 (m, 4H), 1.44 (m, 4H), 1.26 (m, 24H), 0.86 (t, $J = 6.8$ Hz, 6H) ^{13}C NMR (126 MHz, $CDCl_3$) δ (ppm) 159.52, 159.12, 151.60, 151.64, 141.24, 139.20, 139.05, 139.01, 137.25, 136.42, 131.74, 130.35, 129.17, 129.12, 129.05, 126.95, 125.95, 125.68, 125.38, 123.16, 123.03, 117.24, 116.82, 115.39, 115.28, 68.50, 68.11, 32.05, 32.02, 29.64, 29.50, 29.50, 29.40, 29.27, 26.25, 26.08, 22.60, 22.50, 14.29. Calculated for $C_{83}H_{95}N_4O_4S_3$ C, 76.17; H, 7.32; N, 4.28; O, 4.89; S, 7.35, Found C, 76.03; H, 7.86; N, 4.21; S, 7.04.

4.3. Synthesis of B3–B8

The synthesis of compounds **B3–B8** was carried out by dissolving 1.0 mmol of **A3-A8** in 40–80 mL of warm 1,2-dichlorobenzene, adding 2.0 mmol of NBS and stirring the reaction mixture at 60 °C for 1 h. Following concentration of the reaction mixture to dryness and washing the residue with methanol produced pure **B3–B8** in 90–96% yield.

B3 (2,5-bis(7-(5-bromothiophen-2-yl)-5,6-bis(octyloxy)benzo[c][1,2,5]thiadiazol-4-yl)thiophene): ^{1}H NMR ($CDCl_3$, 500 MHz): δ (ppm) 8.59 (s, 2H), 8.40 (d, $J = 4.1$ Hz, 2H), 7.19 (d, $J = 4.1$ Hz, 2H), 4.20 (t, $J = 4.2$ Hz, 4H), 4.15 (t, $J = 4.2$ Hz, 4H), 1.99 (m, 8H), 1.46 (m, 8H), 1.39–1.23 (m, 36H), 0.91 (t, $J = 6.7$ Hz, 6H), 0.83 (t, $J = 6.9$ Hz, 6H) ^{13}C NMR (126 MHz, $CDCl_3$) δ (ppm) 152.09, 151.99, 151.20, 150.61, 136.36, 136.08, 131.01, 130.84, 129.81, 118.22, 116.86, 115.43, 74.68, 74.63, 32.00, 30.57, 30.51, 29.80, 29.69, 29.49, 29.48, 26.17, 22.85, 22.80, 14.28, 14.22. Calculated for $C_{56}H_{74}Br_2N_4O_4S_5$ C, 56.65; H, 6.28; Br, 13.46; N, 4.72; O, 5.39; S, 13.50, Found C, 56.61; H, 6.56; Br, 13.10; N, 4.78; S, 13.56.

B4 (2,5-bis(7-(5-bromothiophen-2-yl)-2-(decyl)-2H-benzo[d][1,2,3]triazol-4-yl)thiophene):^{1}H NMR ($CDCl_3$, 500 MHz): δ (ppm) 8.20 (s, 2H), 7.81 (d, $J = 5$ Hz, 2H), 7.68 (d, $J = 7.6$ Hz, 2H), 7.56 (d, $J = 7.6$ Hz, 2H), 7.14 (d, $J = 3.9$ Hz, 2H), 4.84 (t, $J = 7.2$ Hz, 4H), 2.21 (m, 2H), 1.44 (m, 4H), 1.26 (m, 24H), 0.86 (t, $J = 6.8$ Hz, 6H) ^{13}C NMR (126 MHz, $CDCl_3$) δ (ppm) 142.18, 141.98, 141.60, 140.10, 131.03, 128.79, 126.96, 124.04, 122.88, 122.79, 122.51, 113.17, 57.09, 32.03, 30.23, 29.68, 29.62, 29.44, 29.21, 26.77, 22.82, 14.26 Calculated for $C_{44}H_{52}Br_2N_6S_3$: C, 57.39; H, 5.69; Br, 17.35; N, 9.13; S, 10.44, Found: C, 57.45; H, 5.97; Br, 17.18; N, 8,56; S, 10.84.

B5 (2,5-bis(7-(5-bromothiophen-2-yl)-2-(2-ethylhexyl)-2H-benzo[d][1,2,3]triazol-4-yl)thiophene): ^{1}H NMR ($CDCl_3$, 500 MHz): δ (ppm) 8.19 (s, 2H), 7.80 (d, $J = 5$ Hz, 2H), 7.66 (d, $J = 7.6$ Hz, 2H), 7.53 (d, $J = 7.6$ Hz, 2H), 7.12 (d, $J = 3.9$ Hz, 2H), 4.84 (t, $J = 7.2$ Hz, 4H), 2.22 (m, 2H), 1.44 (m, 4H), 1.26 (m, 24H), 0.86 (t, $J = 6.8$ Hz, 6H) ^{13}C NMR ($CDCl_3$, 126 MHz) δ(ppm) 142.04, 141.85, 141.47, 139.96, 130.89, 128.66, 126.83, 123.91, 122.75, 122.65, 122.38, 113.03, 56.96, 31.89, 30.09, 29.72, 29.54, 29.07, 26.63, 22.96, 14.12. Calculated for $C_{40}H_{44}Br_2N_6S_3$: C, 55.55; H, 5.13; Br, 18.48; N, 9.72; S, 11.12, Found: C, 55.76; H, 5.84; Br, 17.35; N, 10.02; S, 11.03.

Compound **B6** (2,5-bis(8-(5-bromothiophen-2-yl)quinoxalin-5-yl)thiophene) is not soluble in organic solvents, therefore its characterisation with NMR spectroscopy was not possible. FT-IR (KBr): 3425, 1647, 1555, 1458, 1419, 1377, 1349, 1280, 1186, 1143, 1081, 1059, 1017, 968, 945, 863, 835, 789, 667, 545, 490 Calculated for $C_{28}H_{14}Br_2N_4S_3$: C, 50.77; H, 2.13; Br, 24.12; N, 8.46; S, 14.52, Found: C, 50.43; H, 2.86; Br, 24.50; N, 8.43; S, 13.78.

B7 (2,5-bis(8-(5-bromothiophen-2-yl)-2,3-diphenylquinoxalin-5-yl)thiophene): ^{1}H NMR ($CDCl_3$, 500 MHz): δ (ppm) 8.01–7.99 (m, 4H), 7.91 (s, 2H), 7.71 (d, $J = 6.4$ Hz, 4H), 7.62 (d, $J = 7.2$ Hz, 4H), 7.50 (s, 2H), 7.41 (m, 8H), 7.29 (m, 2H), 7.22–7.20 (m, 2H), 7.08 (d, $J = 3.7$ Hz, 2H), ^{13}C NMR ($CDCl_3$, 126 MHz): δ (ppm) 151.97, 151.79, 141.53, 139.91, 138.67, 138.50, 137.60, 136.83, 131.77, 130.63, 130.58, 130.42, 129.35, 129.27, 129.21, 129.00, 128.44, 128.29, 127.55, 127.02, 125.91, 125.55, 117.07 Calculated for $C_{51}H_{29}Br_2N_4S_3$ (%): C, 64.22; H, 3.06; Br, 16.75; N, 5.87; S, 10.08, Found C, 64.59; H, 3.49; Br, 16.38; N, 5.11; S, 10.43.

B8 (2,5-bis(8-(5-bromothiophen-2-yl)-2,3-bis(3-(octyloxy)phenyl)quinoxalin-5-yl)thiophene): ^{1}H NMR ($CDCl_3$, 500 MHz): δ (ppm) 8.05 (m, 4H), 7.85 (s, 2H), 7.61 (dd, $J = 3.4$, 2.3 Hz, 2H), 7.52 (d, $J = 4.1$ Hz, 4H), 7.43 (dd, $J = 3.4$, 2.3 Hz, 2H), 7.22 (t, 2H, $J = 7.9$ Hz), 7.14 (m, 2H), 7.11 (d, $J = 4$ Hz, 2H), 7.08 (m, 2H), 7.02–6.98 (m, 4H), 6.77 (m, 2H), 4.06 (t, $J = 6$ Hz, 4H), 3.60 (t, $J = 6$ Hz, 4H), 1.82 (m, 4H), 1.51 (m, 4H), 1.31 (m, 20H) 1.19 (m, 4H), 1.08 (m, 8H), 0.99 (m, 4H), 0.90 (t, $J = 7.1$ Hz, 6H), 0.83 (t, $J = 7.3$ Hz, 6H) ^{13}C NMR ($CDCl_3$, 126 MHz): δ (ppm) 159.54, 159.18, 151.79, 151.641, 141.84, 139.77, 139.72, 139.64, 137.26, 136.50, 131.76, 130.36, 129.16, 129.10, 129.00, 126.99, 129.94, 125.69, 125.32, 123.16, 123.00, 117.26, 116.82, 115.39, 115.28, 68.50, 68.11, 32.05, 32.02, 29.64, 29.57, 29.50, 29.45, 29.28, 26.39, 26.08, 22.88, 22.85, 14.31 Calculated for $C_{83}H_{93}Br_2N_4O_4S_3$ (%): C, 67.97; H, 6.39; Br, 10.90; N, 3.82; O, 4.36; S, 6.56, Found C, 68.06; H, 6.61; Br, 10.72; N, 3.71; S, 6.48.

4.4. Synthesis of C3, C4, C5 and C8

Synthesis was performed according to the previously described

procedure [20]. Compound **B3**, **B4**, **B5** or **B8** (0.43 mmol), 2-(tributylstannyl)thiophene (0.650 g, 1.76 mmol) and $Pd(PPh_3)_4$ (0.020 g,0.02 mmol) were dissolved in 50 mL of toluene, deaerated and heated at reflux for 6 h. Then the solvent was removed at the rotary evaporator and the residue was washed with ethanol. Compounds were purified by preparative GPC. The yield of **C3**, **C4**, **C5** and **C8** varied from 85% to 92%

4.5. Synthesis of C6, C7

Compounds **C6** and **C7** were prepared following the previously reported procedure [12]. Compound **B6** or **B7** (2 mmol) and (3-(2-hexyldecyl)thien-2-yl)boronic acid (2.6 g, 5.0 mmol) were placed under argon in a two-necked round-bottom flask equipped with a reflux condenser. Afterwards, the toluene (50 mL), 2 M aqueous solution of K_2CO_3 (2 mL), aliquat 336 (1 drop, ca. 80 mg), and tetrakis (triphenylphosphine)palladium (0) (10 mg) were added in the listed here sequence. The obtained reaction mixture was stirred vigorously at 40–50 °C. The course of the reaction was monitored by HPLC. The synthesis was terminated when the starting compound disappeared and the amount of the monofunctionalization product was below 5%. The mixture was poured into water and extracted with chloroform. The organic layer was then dried over anhydrous $MgSO_4$. Finally, the solvent was removed at the rotary evaporator, producing a viscous oily residue. The crude product was dissolved in 40 mL of toluene and filtered through a syringe filter (PTFE, 0.45 μm). The solution was processed further using a preparative Shodex GPC column (20 mm × 250 mm) and toluene as eluent which resulted in isolation of pure compound with the yield of 56–60%.

C3 (2,5-bis(7-([2,2′-bithiophen]-5-yl)-5,6-bis(octyloxy)benzo[c][1,2,5]thiadiazol-4-yl)thiophene): ^{1}H NMR ($CDCl_3$, 500 MHz): δ (ppm) 8.61 (s, 2H), 8.54 (d, J = 3.9 Hz, 2H), 7.31 (m, 4H), 7.27 (d, J = 6.1 Hz, 2H), 7.08 (dd, J = 5.1 Hz, J = 3.6 Hz, 2H), 4.21 (m, 8H), 2.06 (m, 8H), 1.51 (m, 8H), 1.41–1.21 (m, 36H), 0.90 (t, J = 6.7 Hz, 6H), 0.85 (t, J = 6.9 Hz, 6H) ^{13}C NMR ($CDCl_3$, 126 MHz): δ (ppm) 152.26, 151.94, 151.27, 150.95, 138.97, 137.76, 136.41, 133.42, 131.76, 130.73, 129.17, 128.36, 128.07, 125.43, 124.75, 123.86, 123.71, 117.93, 117.44, 74.67, 74.59, 32.01, 30.61, 29.50, 29.29, 29.20, 22.853, 22.81, 14.25, 14.22. Calculated for $C_{64}H_{80}N_4O_4S_7$ (%): C, 64.39; H, 6.75; N, 4.69; O, 5.36; S, 18.80. Found: C, 64.78; H, 7.03; N, 4.37; S, 19.04.

C4 (2,5-bis(7-([2,2′-bithiophen]-5-yl)-2-(decyl)-2H-benzo[d][1,2,3]triazol-4-yl)thiophene): ^{1}H NMR ($CDCl_3$, 500 MHz): δ (ppm) 8.19 (s, 2H), 8.01 (d, J = 3.8 Hz, 2H), 7.65 (d, J = 7.6 Hz, 2H), 7.59 (d, J = 7.6 Hz, 2H), 7.27 (m, 2H), 7.25 (m, 4H),7.05 (m, 2H) 4.83 (t, J = 7.2 Hz, 4H), 2.22 (m, 4H), 1.43 (m, 8H), 1.26 (m, 20H), 0.87 (t, J = 7.5 Hz, 6H); ^{13}C NMR ($CDCl_3$, 126 MHz) δ (ppm) 142.17, 142.10, 140.08, 138.97, 137.66, 137.54, 128.05, 124.88, 124.66, 123.96, 123.64, 123.39, 122.82, 122.57, 57.00, 32.03, 30.23, 29.70, 29.64, 29.46, 29.24, 26.80, 22.83, 14.26. Calculated for $C_{52}H_{58}N_6S_5$: C, 67.35; H, 6.30; N, 9.06; S, 17.29, Found: C, 67.12; H, 6.86; N, 9.24; S, 16.78.

C5 (2,5-bis(7-([2,2′-bithiophen]-5-yl)-2-(2-ethylhexyl)-2H-benzo[d][1,2,3]triazol-4-yl)thiophene): ^{1}H NMR ($CDCl_3$, 500 MHz): δ (ppm) 8.21 (s, 2H), 8.03 (d, J = 3.8 Hz, 2H), 7.69 (d, J = 7.6 Hz, 2H), 7.62 (d, J = 7.6 Hz, 2H), 7.27 (m, 2H), 7.25 (m, 4H), 7.08 (m, 2H) 4.78 (d, J = 6.6 Hz, 4H), 2.31 (m, 4H), 1.44–1.34 (m, 16H), 1.01 (t, J = 7.5 Hz, 6H), 0.93 (t, J = 7.5 Hz, 6H); ^{13}C NMR ($CDCl_3$, 126 MHz) δ (ppm) 142.14, 142.07, 140.14, 139.04, 137.59, 128.70, 128.07, 128.00, 124.92, 124.70, 123.98, 123.69, 123.44, 122.77, 122.52. . Calculated for $C_{48}H_{50}N_6S_5$: C, 66.17; H, 5.78; N, 9.65; S, 18.40, Found: C, 66.42; H, 6.12; N, 9.43; S, 18.03.

C6 (2,5-bis(8-(3'-(2-ethylhexyl)-[2,2′-bithiophen]-5-yl)quinoxalin-5-yl)thiophene): ^{1}H NMR ($CDCl_3$, 500 MHz): δ (ppm) 9.01 (d, J = 22.6 Hz, 4H), 8.20 (m, 4H), 7.93 (s, 2H), 7.81 (d, J = 3.8 Hz, 2H), 7.21 (m, 4H), 6.94 (d, J = 5.2 Hz, 2H), 2.08 (d, J = 7.2 Hz, 4H), 1.73 (m, 2H), 1.38–1.26 (m, 16H), 0.90–0.84 (m, 12H) ^{13}C NMR ($CDCl_3$, 126 MHz) δ (ppm) 152.30, 151.91, 147.60, 147.56, 139.76, 139.07, 138.60, 137.04, 131.09, 130.80, 129.85, 129.70, 127.23, 126.55, 125.44, 124.33, 122.25, 120.81, 40.31, 33.80, 32.75, 28.90, 25.90, 23.25, 14.33, 10.92. Calculated for $C_{52}H_{52}N_4S_5$: C, 69.92; H, 5.87; N, 6.27; S, 17.94, Found: C, 70.11; H, 5.36; N, 6.51; S, 18.02.

C7 (2,5-bis(8-(3'-(2-ethylhexyl)-[2,2′-bithiophen]-5-yl)-2,3-diphenylquinoxalin-5-yl)thiophene):^{1}H NMR ($CDCl_3$, 500 MHz): δ (ppm) 8.11 (s, 2H), 7.97 (s, 2H), 7.83 (d, J = 3.9 HZ, 2H), 7.79–7.77 (m, 4H), 7.67–7.66 (m, 4H), 7.40–7.38 (m, 6H), 7.30–7.28 (m, 4H), 7.25–7.22 (m, 6H), 7.20 (d, J = 3.8 Hz, 2H), 6.97 (d, J = 5.2 Hz, 2H), 2.88 (d, J = 6 Hz, 4H), 1.70 (m, 2H), 1.35–1.22 (m, 16H), 0.83 (t, J = 7.3 Hz, 12H) ^{13}C NMR ($CDCl_3$, 126 MHz) δ (ppm) 151.75, 151.58, 141.65, 139.94, 138.87, 138.79, 138.75, 138.47, 137.68, 137.23, 131.98, 131.53, 131.07, 130.83, 130.66, 130.57, 129.12, 128.92, 128.35, 128.28, 127.35, 127.13, 126.72, 126.53, 125.78, 123.71, 40.48, 33.70, 32.75, 28.88, 25.91, 23.22, 14.28, 10.94. Calculated for $C_{75}H_{67}N_4S_5$: C, 76.04; H, 5.70; N, 4.73; S, 13.53, Found: C, 76.39; H, 5.96; N, 4.57; S, 13.08.

C8 (2,5-bis(8-([2,2′-bithiophen]-5-yl)-2,3-bis(3-(octyloxy)phenyl) quinoxalin-5-yl)thiophene): ^{1}H NMR ($CDCl_3$, 500 MHz): δ (ppm) 8.13 (s, 4H), 7.92 (s, 2H), 7.78 (d, J = 4 Hz, 2H), 7.60 (s, 2H), 7.47 (s, 2H), 7.29 (d, J = 3.5 Hz, 2H), 7.25 (d, J = 4.1 Hz, 4H), 7.10–6.96 (m, 12H), 6.77 (m, 2H), 3.96 (t, J = 6 Hz, 4H), 3.62 (t, J = 6 Hz, 4H), 1.73 (m, 4H), 1.60 (m, 4H), 1.39–0.98 (m, 40H), 0.89 (t, J = 7.1 Hz, 6H), 0.80 (t, J = 7.3 Hz, 6H)^{13}C NMR ($CDCl_3$, 126 MHz) δ (ppm) 159.41, 159.17, 151.60, 151.48, 141.92, 140.81, 139.99, 139.69, 138.07, 137.55, 137.38, 136.87, 131.55, 130.95, 129.13, 128.97, 128.02, 127.06, 126.88, 126.84, 126.32, 124.52, 123.60, 123.41, 123.16, 122.98, 116.84, 116.52, 115.87, 115.31, 68.36, 68.11, 32.01, 29.60, 29.54, 29.48, 29.45, 29.26, 26.24, 26.06, 22.84, 22.83, 14.28, 14.26 Calculated for $C_{91}H_{99}N_4O_4S_5$: C, 74.20; H, 6.77; N, 3.80; O, 4.34; S, 10.88, Found: C, 74.02; H, 6.31; N, 3.08; S, 10.75.

4.6. Synthesis of D3-D8

The synthesis of compounds **D3-D8** was carried out by dissolving 1.0 mmol of **A3-A8** in 40–80 mL of warm 1,2-dichlorobenzene, adding 2.0 mmol of NBS and stirring the reaction mixture at 40 °C for 1 h. Following concentration of the reaction mixture to dryness and washing the residue with methanol produced pure **D3-D8** in 90–96% yield.

D3 (2,5-bis(7-(5′-bromo-[2,2′-bithiophen]-5-yl)-5,6-bis(octyloxy)benzo[c][1,2,5]thiadiazol-4-yl)thiophene):^{1}H NMR ($CDCl_3$, 500 MHz): δ (ppm) 8.61 (s, 2H), 8.52 (d, J = 3.9 Hz, 2H), 7.23 (d, J = 4 Hz, 2H), 7.02 (m, 4H), 4.19 (m, 8H), 2.01 (m, 8H)1.51 (m, 8H), 1.08–1.23 (m, 36H), 0.89 (t, J = 6.7 Hz, 6H), 0.84 (t, J = 6.9 Hz, 6H) ^{13}C NMR ($CDCl_3$, 126 MHz): δ (ppm) 152.22, 152.07, 151.25, 150.88, 139.28, 137.82, 136.44, 133.91, 131.74, 130.92, 130.82, 123.91, 123.88, 118.12, 117.22, 111.35, 74.73, 74.62, 32.02, 30.64, 30.61, 29.82, 29.77, 29.52, 29.51, 26.29, 26.20, 22.87, 22.81, 14.27, 14.23 Calculated for $C_{64}H_{78}Br_2N_4O_4S_7$ (%): C 56.87; H 5.82; Br 11.82; N 4.15; O 4.73; S 16.60. Found: C 56.67; H 5.15; Br 11.44; N 4.58; S 16.03.

D4 (2,5-bis(7-(5′-bromo-[2,2′-bithiophen]-5-yl)-2-(decyl)-2H-benzo[d][1,2,3]triazol-4-yl)thiophene): ^{1}H NMR ($CDCl_3$, 500 MHz): δ (ppm) 8.50 (s, 2H), 8.39 (d, J = 3.3 Hz, 2H), 7.66 (d, J = 3.2 Hz, 2H), 7.54 (d, J = 3.4 Hz, 2H), 7.21 (m, 4H), 7.01 (d, J = 3.4, 2H), 4.81 (t, J = 6 Hz, 4H), 2.20 (m 4H), 1.40 (m, 8H), 1.23 (m, 16H), 0.84 (t, J = 7.1 Hz, 6H) ^{13}C NMR ($CDCl_3$, 126 MHz): δ (ppm) 142.20, 141.91, 141.62, 140.12, 131.10, 130.60, 129.15, 128.92, 128.75, 128.34, 128.25, 127.43, 127.03, 126.54, 126.11, 110.41, 57.07, 32.08, 30.21, 29.69, 29.64, 29.43, 29.22, 26.76, 22.85, 14.24 Calculated for $C_{52}H_{56}Br_2N_6S_5$ (%): C, 57.56; H, 5.20; Br, 14.73; N, 7.74; S, 14.77. Found: C, 57.86; H, 5.49; Br, 14.71; N, 7.82; S, 14.12.

D5 (2,5-bis(7-(5′-bromo-[2,2′-bithiophen]-5-yl)-2-(2-ethylhexyl)-2H-benzo[d][1,2,3]triazol-4-yl)thiophene): ^{1}H NMR ($CDCl_3$, 500 MHz): δ (ppm) 8.52 (s, 2H), 8.37 (d, 2H), 7.65 (d, J = 3.4 Hz, 2H), 7.53 (d, J = 3.1 Hz, 2H), 7.21 (m, 4H), 7.05 (d, J = 3.4 Hz, 2H), 4.75 (d, J = 7.2 Hz, 4H), 2.32 (m, 2H), 1.40 (m, 4H), 1.29 (m, 12H), 1.02 (t, J = 6.8 Hz, 6H), 0.95 (t, J = 6.8 Hz, 6H) ^{13}C NMR ($CDCl_3$, 126 MHz): δ (ppm) 142.17,

142.00, 141.58, 140.08, 131.05, 130.53, 129.23, 128.92, 128.78, 128.37, 128.25, 127.45, 127.03, 126.55, 126.13, 110.41, 56.61, 31.85, 30.01, 29.69, 29.05, 26.61, 22.94, 14.11 Calculated for $C_{48}H_{48}Br_2N_6S_5$ (%): C, 56.02; H, 4.70; Br, 15.53; N, 8.17; S, 15.58. Found: C, 56.87; H, 5.07; Br, 14.73; N, 8.07; S, 15.26.

D6 (2,5-bis(8-(5′-bromo-3'-(2-ethylhexyl)-[2,2′-bithiophen]-5-yl) quinoxalin-5-yl)thiophene): ^{1}H NMR ($CDCl_3$, 500 MHz): δ 9.05 (d, J = 22.4 Hz, 4H), 8.23 (m, 4H), 7.95 (s, 2H), 7.36 (d, J = 7.4 Hz, 2H), 6.99 (d, J = 7.0 Hz, 2H), 6.84 (s, 2H), 2.10 (d, J = 70 Hz, 4H), 1.75 (m, 2H), 1.35–1.23 (m, 16H), 0.91–0.83 (m, 12H) ^{13}C NMR ($CDCl_3$, 126 MHz): δ (ppm) 152.03, 151.68, 147.51, 140.37, 139.09, 137.47, 137.10, 133.56, 132.31, 129.94, 129.58, 127.54, 126.47, 125.58, 122.03, 121.02, 120.95, 111.39, 40.30, 33.78, 32.69, 28.87, 25.82, 23.23, 14.33, 10.90 Calculated for $C_{52}H_{50}Br_2N_4S_5$ (%): C, 59.42; H, 4.79; Br, 15.20; N, 5.33; S, 15.25. Found: C, 59.21; H, 5.02; Br, 15.73; N, 5.29; S, 14.76.

D7 (2,5-bis(8-(5′-bromo-3'-(2-ethylhexyl)-[2,2′-bithiophen]-5-yl)-2,3-diphenylquinoxalin-5-yl)thiophene): ^{1}H NMR ($CDCl_3$, 500 MHz): δ (ppm) 8.08 (s, 2H), 7.95 (s, 2H), 7.77–7.74 (m, 6H), 7.65 (d, J = 7.2 Hz, 4H), 7.41–7.36 (m, 6H), 7.30–7.28 (m, 4H), 7.24–7.21 (m, 2H), 7.12 (d, J = 3.8 Hz, 2H), 6.90 (s, 2H), 6H) 2.73 (d, J = 6 Hz, 4H), 1.62 (m, 2H), 1.34–1.21 (m, 16H), 0.82–0.79 (m, 12H) ^{13}C NMR ($CDCl_3$, 126 MHz): δ (ppm) 151.81, 151.65, 141.65, 139.52, 138.95, 138.74, 138.68, 138.49, 137.66, 137.16, 133.55, 133.32, 131.68, 130.61, 130.57, 129.19, 128.96, 128.38, 128.29, 127.43, 127.08, 126.57, 126.13, 110.42, 40.47, 33.64, 32.66, 28.84, 25.81, 23.18, 14.27, 10.91. Calculated for $C_{75}H_{65}Br_2N_4S_5$ (%): C, 67.10; H, 4.88; Br, 11.90; N, 4.17; S, 11.94. Found: C, 66.93; H, 5.11; Br, 11.74; N, 4.19; S, 12.03.

D8 (2,5-bis(8-(5′-bromo-[2,2′-bithiophen]-5-yl)-2,3-bis(3-(octyloxy) phenyl)quinoxalin-5-yl)thiophene): ^{1}H NMR ($CDCl_3$, 500 MHz): δ (ppm) 7.99 (s, 4H), 7.82 (s, 2H), 7.63 (d, J = 4.1 Hz, 2H), 7.57 (dd, J = 3.4, 2.3 Hz, 4H), 7.41 (dd, J = 3.4, 2.3 Hz, 2H), 7.22 (t, 2H, J = 7.9 Hz), 7.17 (m, 2H), 7.10 (d, J = 4 Hz, 2H), 7.06 (m, 2H), 7.01–6.96 (m, 8H), 6.76 (m, 2H), 3.95 (t, J = 6 Hz, 4H), 3.590 (t, J = 6 Hz, 4H), 1.75 (m, 4H), 1.51 (m, 4H), 1.40 (m, 20H) 1.17 (m, 4H), 1.08 (m, 8H), 0.89 (t, J = 7.1 Hz, 6H), 0.80 (t, J = 7.3 Hz, 6H) ^{13}C NMR ($CDCl_3$, 126 MHz): δ (ppm) 159.41, 159.13, 151.50, 151.36, 139.92, 139.64, 137.86, 137.27, 136.70, 131.54, 130.83, 130.51, 129.07, 128.95, 126.93, 126.60, 126.21, 123.50, 123.42, 123.16, 122.97, 116.73, 116.37, 115.95, 115.38, 111.02, 68.38, 68.10, 32.04, 32.01, 29.65, 29.56, 29.55, 29.49, 29.45, 29.27, 26.30, 26.08, 22.86, 22.82, 14.29, 14.27 Calculated for $C_{91}H_{97}Br_2N_4O_4S_5$ (%): C, 67.02; H, 6.00; Br, 9.80; N, 3.44; O, 3.92; S, 9.83. Found: C, 67.24; H, 5.82; Br, 10.04; N, 3.69; S, 9.31.

Synthesis of P3 (poly [(9-(heptadecan-9-yl)-9H-carbazole)-alt-(2,5-bis(7-([2,2′-bithiophen]-5-yl)-5,6-bis(octyloxy)benzo[c][1,2,5]thiadiazol-4-yl)thiophene)]), **P4** (poly [(9-(heptadecan-9-yl)-9H-carbazole)-alt-(2,5-bis(7-([2,2′-bithiophen]-5-yl)-2-(decyl)-2H-benzo[d][1,2,3]triazol-4-yl)thiophene)]), **P5** (poly [(9-(heptadecan-9-yl)-9H-carbazole)-alt-(2,5-bis(7-([2,2′-bithiophen]-5-yl)-2-(2-ethylhexyl)-2H-benzo[d][1,2,3]triazol-4-yl)thiophene)]), **P6** (poly [(9-(heptadecan-9-yl)-9H-carbazole)-alt-(2,5-bis(8-(3'-(2-ethylhexyl)-[2,2′-bithiophen]-5-yl)quinoxalin-5-yl)thiophene)]), **P7** (poly [(9-(heptadecan-9-yl)-9H-carbazole)-alt-(2,5-bis(8-(3'-(2-ethylhexyl)-[2,2′-bithiophen]-5-yl)-2,3-diphenylquinoxalin-5-yl)thiophene)]), **P8** (poly [(9-(heptadecan-9-yl)-9H-carbazole)-alt-(2,5-bis(8-([2,2′-bithiophen]-5-yl)-2,3-bis(3-(octyloxy)phenyl)quinoxalin-5-yl)thiophene)])

Monomers **5** (143 mg, 0.22 mmol) and **D3-D8** (0.22 mmol) were introduced into reaction and worked up under previously described conditions [12]. The total yield of the purified polymers **P3**–**P8** varied between 50 and 70% depending on the initial molecular weight.

4.7. Computational methodology

All computations were carried out in Gaussian 09 program suite [33]. Density Functional Theory (DFT) and time-dependent DFT (TDDFT) frameworks [34] have been used for calculations of ground and excited state electronic properties, respectively. CAM-B3LYP density functional [35] combined with the 6-31G* basis set was used as a default method. CAM-B3LYP is a long-range corrected hybrid functional known to provide a correct description of electronic excitations and charged states of extended π-conjugated systems [36–38], while 6-31G* basis set usually allows to obtain adequate estimations for geometry and energy parameters for relatively large molecules consisting of the first and second row elements in a substantially short computing time [39,40]. The solvent effects were taken into account using the conductor-like polarizable continuum model [41–43], (CPCM) with the dielectric constant ε_{static} = 4.7 (chloroform) close to upper limit of typical dielectric environment of bulk conjugated polymers [44]. All structures used for calculations of energy parameters have been optimized with a constraint of a planar conduction backbone as a model of a statistically averaged conformation (with removed aliphatic substituents). For some structures, geometry optimizations without this constraint were also performed. For "shorter" (15 aromatic rings in conjugated backbone) and "longer" (25 rings) oligomers (Fig. S7) a number of single point calculations, including those of harmonic vibrational frequencies, IP, EA, vertical electronic excitation energies, natural bond orbitals in vacuum and in chloroform were carried out. Values for dihedrals were chosen to a) correspond to the lowest-energy planar configuration for the dimer (Table S4) and b) form a linear polymer chain fragment c) not introduce considerable steric hindrance effects (because of that, the planar configuration chosen for **P7-8** polymers was sinuous rather than linear). Discrepancy introduced by choosing different planar configuration (if it is not sterically prohibited) for these systems typically does not exceed 40 meV. Also, electronic absorption spectra were modeled using TD-DFT results and gaussian broadening (Fig. S8).

4.8. Cyclic voltammetry measurements

The cyclic voltammetry measurements were performed for thin films (150–250 nm thick) of polymers **P3**–**P8** deposited on a glassy carbon disc electrode (working electrode, d = 5 mm, BAS Inc.) by drop casting from 1,2-dichlorobenzene. The measurements were performed in a three-electrode electrochemical cell using 0.1 M solution of Bu_4NPF_6 (TBAP) in acetonitrile as a supporting electrolyte, platinum wire as a counter electrode and a silver wire immersed in 0.01 M solution of $AgNO_3$ in 0.1 M TBAP (CH_3CN) as a reference Ag/Ag^+ electrode (BAS Inc.). Ferrocene was used as an internal reference. The electrolyte solution was purged with argon before the measurements. The voltammograms were recorded using an ELINS P-30SM instrument at room temperature with a potential sweep rate of 50 mV s^{-1}.

4.9. Fabrication and characterization of photovoltaic devices

General description of fabrication was published previously [19]. Detailed conditions (solvent, additives, donor-acceptor ratio, annealing regimes) are provided in Table 2.

The current–voltage (I–V) characteristics of the devices were obtained in the dark and under simulated 100 mW cm^{-2} AM1.5G illumination conditions provided by a KHS Steuernagel solar simulator integrated in the MBraun glove box. The intensity of the illumination was checked every time before the measurements using a calibrated silicon diode with a known spectral response. The I–V curves were recorded in an inert atmosphere using Advantest 6240A source-measurement units. The EQE spectra were measured under argon atmosphere using a specially designed setup, LOMO instruments, Russia.

CRediT authorship contribution statement

Irina V. Klimovich: Visualization, Investigation, Writing - original draft. **Fedor A. Prudnov:** Data curation, Investigation. **Olga Mazaleva:** Software. **Nikita V. Tukachev:** Software, Visualization. **Alexander V. Akkuratov:** Investigation, Resources. **Ilya V. Martynov:** Investigation. **Alexander S. Peregudov:** Investigation, Resources. **Alexander F.**

Shestakov: Software, Validation. **Andriy Zhugayevych:** Software, Methodology. **Pavel A. Troshin:** Supervision, Writing - review & editing.

Declaration of competing interest

The authors declare that they have no known competing financial interests or personal relationships that could have appeared to influence the work reported in this paper.

Acknowledgements

This work was supported by Russian Science Foundation (grant No.18-13-00205). We acknowledge the contribution of Dr. Liana Inasaridze with electrochemical characterization of some polymers. We also thank Mr. Filipp Obrezkov and Prof. J. Grazulevicius of Kaunas University of Technology for performing photoelectron spectroscopy measurements for polymer films.

Appendix A. Supplementary data

Supplementary data to this article can be found online at https://doi.org/10.1016/j.dyepig.2020.108899.

References

[1] Fu H, Wang Z, Sun Y. Polymer donors for high-performance non-fullerene organic solar cells. Angew Chem Int Ed 2019;58:44422. https://doi.org/10.1002/anie.201806291.
[2] Subramanian KM, Pandian KK. How to design donor – acceptor based heterocyclic conjugated polymers for applications from organic electronics to sensors. Springer International Publishing; 2019. https://doi.org/10.1007/s41061-019-0237-4.
[3] Holliday S, Li Y, Luscombe CK. Progress in Polymer Science Recent advances in high performance donor-acceptor polymers for organic photovoltaics. Prog Polym Sci 2017;70:34–51. https://doi.org/10.1016/j.progpolymsci.2017.03.003.
[4] Li G, Xiaoyuan Z, Fuqiang S, Yue J, Yiping Z, Ping L. Oligothiophene derivatives in organic photovoltaic devices. Prog Chem 2015;27:1435–47.
[5] Jung JW, Jo JW, Jung EH, Jo WH. Recent progress in high ef fi ciency polymer solar cells by rational design and energy level tuning of low bandgap copolymers with various electron-withdrawing units. Org Electron 2016;31:149–70. https://doi.org/10.1016/j.orgel.2016.01.034.
[6] Xiao Z, Jia X, Ding L. Ternary organic solar cells offer 14% power conversion efficiency. Sci Bull 2017;62:1562–4. https://doi.org/10.1016/j.scib.2017.11.003.
[7] Zhao J, Li Y, Yang G, Jiang K, Lin H, Ade H, et al. Efficient organic solar cells processed from hydrocarbon solvents. Nat Energy 2016;1:15027. https://doi.org/10.1038/nenergy.2015.27.
[8] Liu Y, Zhao J, Li Z, Mu C, Ma W, Hu H, et al. Multiple cases of high-efficiency polymer solar cells. Nat Commun 2014;5:1–8. https://doi.org/10.1038/ncomms6293.
[9] Liu Q, Jiang Y, Jin K, Qin J, Xu J, Li W, et al. 18% Efficiency organic solar cells. Sci Bull 2020;65:272–5. https://doi.org/10.1016/j.scib.2020.01.001.
[10] Brown SJ, Decrescent RA, Nakazono DM, Willenson SH, Ran A, Liu X, et al. Enhancing organic semiconductor-surface plasmon polariton coupling with molecular orientation. Nano Lett 2017;17:6151–6. https://doi.org/10.1021/acs.nanolett.7b02767.
[11] Brus VV, Lee HK, Proctor CM, Ford M, Liu X, Burgers MA, et al. Balance between light absorption and recombination losses in solution-processed small molecule solar cells with normal or inverted structures. Adv Energy Mater 2018:1801807. https://doi.org/10.1002/aenm.201801807.
[12] Akkuratov AV, Susarova DK, Kozlov OV, Chernyak AV, Moskvin YL, Frolova LA, et al. Design of (X-DADAD) n type copolymers for efficient bulk heterojunction organic solar cells. Macromolecules 2015;48:2013–21. https://doi.org/10.1021/ma5023956.
[13] Frolova LA, Piven NP, Susarova DK, Akkuratov AV, Babenko SD, Troshin PA. ESR spectroscopy for monitoring the photochemical and thermal degradation of conjugated polymers used as electron donor materials in organic bulk heterojunction solar cells. Chem Commun 2015;51:2242–4. https://doi.org/10.1039/C4CC08146C.
[14] Akkuratov AV, Kuznetsov IE, Martynov IV, Sagdullina DK, Kuznetsov PM, Ciammaruchi L, et al. What can we learn from model systems: impact of polymer backbone structure on performance and stability of organic photovoltaics. Polymer (Guildf) 2019;183:121849. https://doi.org/10.1016/j.polymer.2019.121849.
[15] Burgués-Ceballos I, Hermerschmidt F, Akkuratov AV, Susarova DK, Troshin PA, Choulis SA. High-performing polycarbazole derivatives for efficient solution-processing of organic solar cells in air. ChemSusChem 2015;8:4209–15. https://doi.org/10.1002/cssc.201501128.
[16] Wang JL, Yin QR, Miao JS, Wu Z, Chang ZF, Cao Y, et al. Rational design of small molecular donor for solution-processed organic photovoltaics with 8.1% efficiency and high fill factor via multiple fluorine substituents and thiophene bridge. Adv Funct Mater 2015;25:3514–23. https://doi.org/10.1002/adfm.201500190.
[17] Privado M, Cuesta V, de la Cruz P, Keshtov ML, Sharma GD, Langa F. Tuning the optoelectronic properties for high-efficiency (>7.5%) all small molecule and fullerene-free solar cells. J Mater Chem A 2017;5. https://doi.org/10.1039/C7TA03815A. 14259–69.
[18] Akkuratov AV, Susarova DK, Inasaridze LN, Troshin PA. The effect of the fluorine loading on the optoelectronic and photovoltaic properties of (X-DADAD-) $_n$ -type donor-acceptor copolymers with the benzothiadiazole A units. Phys Status Solidi Rapid Res Lett 2017;11:1700087. https://doi.org/10.1002/pssr.201700087.
[19] Klimovich IV, Susarova DK, Inasaridze LN, Akkuratov AV, Chernyak AV, Troshin PA. Effect of alkyl side chains on the photovoltaic performance of 2,1,3-benzoxadiazole-based (-X-DADAD-)n-Type copolymers. Macromol Chem Phys 2017;218:1700055.
[20] Klimovich IV, Susarova DK, Prudnov FA, Inasaridze LN, Mukhacheva OA, Chernyak AV, et al. Solubilized 5,6-bis(octyloxy) benzoxadiazole as a versatile acceptor block for designing novel (-X-DADAD-) n and (-X-DADADAD-) n electron donor copolymers for bulk heterojunction organic solar cells. Sol Energy Mater Sol Cells 2016;155:378–86.
[21] Lee MH, Kim J, Kang M, Kim J, Kang B, Hwang H, et al. Precise side-chain engineering of thienylenevinylene-benzotriazole-based conjugated polymers with coplanar backbone for organic field effect transistors and CMOS-like inverters. ACS Appl Mater Interfaces 2017;9:2758–66. https://doi.org/10.1021/acsami.6b14701.
[22] Jo S, Kim D, Son SH, Kim Y, Lee TS. Conjugated poly(fluorene-quinoxaline) for fluorescence imaging and chemical detection of nerve agents with its paper-based strip. ACS Appl Mater Interfaces 2014;6:1330–6. https://doi.org/10.1021/am405430t.
[23] Blouin N, Michaud A, Leclerc M. A low-bandgap poly(2,7-carbazole) derivative for use in high-performance solar cells. Adv Mater 2007;19:2295–300. https://doi.org/10.1002/adma.200602496.
[24] Cardona CM, Li W, Kaifer AE, Stockdale D, Bazan GC. Electrochemical considerations for determining absolute frontier orbital energy levels of conjugated polymers for solar cell applications. Adv Mater 2011;23:2367–71. https://doi.org/10.1002/adma.201004554.
[25] Scharber MC, Mühlbacher D, Koppe M, Denk P, Waldauf C, Heeger AJ, et al. Design rules for donors in bulk-heterojunction solar cells - towards 10 % energy-conversion efficiency. Adv Mater 2006;18:789–94. https://doi.org/10.1002/adma.200501717.
[26] Mumyatov AV, Prudnov FA, Inasaridze LN, Mukhacheva OA, Troshin PA. High LUMO energy pyrrolidinofullerenes as promising electron-acceptor materials for organic solar cells. J Mater Chem C 2015;3:11612–7. https://doi.org/10.1039/C5TC02509E.
[27] Hu Z, Zhong Z, Chen Y, Sun C, Huang F, Peng J, et al. Energy-level alignment at the organic/electrode interface in organic optoelectronic devices. Adv Funct Mater 2016;26:129–36. https://doi.org/10.1002/adfm.201503420.
[28] Ye L, Zhang S, Zhao W, Yao H, Hou J. Highly efficient 2D-conjugated benzodithiophene-based photovoltaic polymer with linear alkylthio side chain. Chem Mater 2014;26:3603–5. https://doi.org/10.1021/cm501513n.
[29] Zhang Y, Sajjad MT, Blaszczyk O, Parnell AJ, Ruseckas A, Serrano LA, et al. Large crystalline domains and an enhanced exciton diffusion length enable efficient organic solar cells. Chem Mater 2019;31:6548–57. https://doi.org/10.1021/acs.chemmater.8b05293.
[30] Yeboah D, Singh J. Study of the contributions of donor and acceptor photoexcitations to open circuit voltage in bulk heterojunction organic solar cells. Electron 2017;6. https://doi.org/10.3390/electronics6040075.
[31] Hörmann U, Lorch C, Hinderhofer A, Gerlach A, Gruber M, Kraus J, et al. Vocfrom a morphology point of view: the influence of molecular orientation on the open circuit voltage of organic planar heterojunction solar cells. J Phys Chem C 2014;118:26462–70. https://doi.org/10.1021/jp506180k.
[32] Ran NA, Roland S, Love JA, Savikhin V, Takacs CJ, Fu YT, et al. Impact of interfacial molecular orientation on radiative recombination and charge generation efficiency. Nat Commun 2017;8:1–9. https://doi.org/10.1038/s41467-017-00107-4.
[33] Frisch MJ, et al. Gaussian 09 2009.
[34] Frisch MJ. Gaussian 09 2009.
[35] Yanai T, Tew DP, Handy NC. A new hybrid exchange-correlation functional using the Coulomb-attenuating method (CAM-B3LYP). Chem Phys Lett 2004;393:51–7. https://doi.org/10.1016/j.cplett.2004.06.011.
[36] Magyar RJ, National LA, Alamos L, Tretiak S, National LA, Alamos L. Dependence of spurious charge-transfer excited states on orbital exchange in TDDFT : large molecules and clusters. J Chem Theory Comput 2007;3:976–87.
[37] Nayyar IH, Batista ER, Tretiak S, Saxena A, Smith DL, Martin RL. Role of geometric distortion and polarization in localizing electronic excitations in conjugated polymers. J Chem Theory Comput 2013;9:1144–54. https://doi.org/10.1021/ct300837d.
[38] Zhugayevych A, Postupna O, Bakus II RC, Welch GC, Bazan GC, Tretiak S. Ab initio study of a molecular crystal for photovoltaics: light absorption, exciton and charge carrier transport. J Phys Chem C 2013;117:4920–30. https://doi.org/10.1021/jp310855p.
[39] Badaeva E, Harpham MR, Guda R, Süzer Ö, Ma CQ, Bäuerle P, et al. Excited-state structure of oligothiophene dendrimers: computational and experimental study. J Phys Chem B 2010;114:15808–17. https://doi.org/10.1021/jp109624d.
[40] Masunov A, Tretiak S. Prediction of two-photon absorption properties for organic chromophores using time-dependent density-functional theory. J Phys Chem B 2004;108:899–907. https://doi.org/10.1021/jp036513k.

[41] Takano Y, Houk KN. Benchmarking the conductor-like polarizable continuum model (CPCM) for aqueous solvation free energies of neutral and ionic organic molecules. J Chem Theory Comput 2005;1:70–7. https://doi.org/10.1021/ct049977a.
[42] Cossi M, Rega N, Scalmani G, Barone V. Energies, structures, and electronic properties of molecules in solution with the C-PCM solvation model. J Comput Chem 2003;24:669–81. https://doi.org/10.1002/jcc.10189.
[43] Barone V, Cossi M. Conductor solvent model. J Phys Chem A 1998;102:1995–2001. https://doi.org/10.1002/2014JA020863.
[44] Ostroverkhova O. Organic optoelectronic materials: mechanisms and applications. Chem Rev 2016;116:13279–412. https://doi.org/10.1021/acs.chemrev.6b00127.